Sparsity in the Delay-Doppler Domain for Measured 60 GHz Vehicle-to-Infrastructure Communication Channels

Herbert Groll*, Erich Zöchmann*†‡, Stefan Pratschner*†, Martin Lerch*,
Daniel Schützenhöfer*†, Markus Hofer§, Jiri Blumenstein‡, Seun Sangodoyin¶,
Thomas Zemen§, Aleš Prokeš‡, Andreas F. Molisch¶, and Sebastian Caban*†

* Institute of Telecommunications, TU Wien, Austria
† Christian Doppler Laboratory for Dependable Wireless Connectivity for the Society in Motion
‡ Department of Radio Electronics, TU Brno, Czech Republic
§ Center for Digital Safety & Security, AIT Austrian Institute of Technology, Austria
¶ Wireless Devices and Systems Group, University of Southern California, USA

***Abstract*—We report results from millimeter wave vehicle-to-infrastructure (V2I) channel measurements conducted on Sept. 25, 2018 in an urban street environment, down-town Vienna, Austria. Measurements of a frequency-division multiplexed multiple-input single-output channel have been acquired with a time-domain channel sounder at 60 GHz with a bandwidth of 100 MHz and a frequency resolution of 5 MHz. Two horn antennas were used on a moving transmitter vehicle: one horn emitted a beam towards the horizon and the second horn emitted an elevated beam at 15-degrees up-tilt. This configuration was chosen to assess the impact of beam elevation on V2I communication channel characteristics: propagation loss and sparsity of the local scattering function in the delay-Doppler domain. The measurement results within urban speed limits show high sparsity in the delay-Doppler domain.**

***Index Terms*—OTFS, delay-Doppler domain, sparsity, millimeter wave, vehicular communications, channel estimation**

I. Introduction

Vehicular communications was intensely investigated in the last decade [1]–[4]. MmWave have been a research topic in vehicular communications for already several decades [5], [6]. The path loss for train-to-infrastructure scenarios in the millimeter wave (mmWave) frequency band is measured in [5], performance for vehicle-to-vehicle (V2V) communication is investigated in [6].

The effect of an overtaking vehicle on a V2V channel at 60 GHz of a communicating car platoon has been investigated in [7], [8]. A more detailed statistical analysis of delay and Doppler spread is provided in [9], [10]. V2V channel measurements with antennas placed in the bumpers of cars at 38 GHz and 60 GHz, using a channel sounder with 1 GHz bandwidth, have been conducted in [11]. Further mmWave V2V measurements with approaching cars are shown in [12]. Doppler spectra of vehicle-to-infrastructure (V2I) measurements at 28 GHz in an expressway environment are shown in [13]. Doppler spectra of vibrations appearing while the vehicle is in operation are shown in [14] and [15].

The mmWave wireless channel has been observed to have a sparse multipath structure in multiple domains [16]–[18]. For channel estimation using sparse reconstruction, several techniques exist [19]. Sparse channel fits via the least absolute shrinkage and selection operator (LASSO) applied in the delay domain are provided in [20]–[23]. In [22] and [23], Akaike's information criterion was used to select the appropriate sparsity level, where approximately 4 to 6 clusters in the delay domain have been found. Sparse signal reconstruction using the sparse Bayesian learning (SBL) framework with low-complexity is used in [24], [25]. A fixed-point implementation of SBL [25] is shown in [26].

How to exploit the delay-Doppler sparsity of wireless channels is shown in [27]. The orthogonal time frequency space (OTFS) modulation [28] performs especially well for wireless channels with sparsity in the delay-Doppler domain, such as in mmWave communication systems [29].

Our contribution

In this contribution, we show that the sparsity in the delay-Doppler domain holds true for measured 60 GHz V2I communication channels in a street crossing scenario in an urban environment. We estimate the channel and find a representation in the delay-Doppler domain with a multitaper estimator. Furthermore, a sparse estimation with sub-Nyquist sampling in the delay domain is carried out using SBL.

The support for this research by Wien Leuchtet (Magistratsabteilung 33) is gratefully acknowledged. This work was supported in part by the Austrian Federal Ministry for Digital and Economic Affairs, in part by the National Foundation for Research, Technology and Development, in part by the Czech Science Foundation under Project 17-27068S, and in part by the National Sustainability Program under Grant LO1401. The work of S. Sangodoyin and A. F. Molisch was supported in part by NSF under Grant CNS-1457340, and in part by NIST under Grant 70NANB17H157. This work was carried out in the framework of COST Action CA15104 IRACON.

II. Measured Scenario

The measurement scenario and placement of the transmitters (TXs) and the receiver (RX) is shown in Fig. 1a. Our TXs are mounted on the roof rack of a car. The RX is positioned at the crossroads of a street canyon, at 5 m height. We are observing multipath components (MPCs) of the wireless channel during the approach and passage of the moving transmitter vehicle at the crossroads. All MPCs are Doppler shifted proportional to their respective radial velocity.

For our setup, the 60 GHz free space path loss calculates to 100 dB at the maximum distance of interest. Both TXs use horn antennas with a gain of 20 dBi, which point towards driving direction. One horn (TX 0°) emits a beam towards the horizon and the second horn (TX 15°) emits a beam at 15° up-tilt as shown in Fig. 1b. At the receiver side, an omni-directional $\lambda/4$ monopole antenna is used. The receive antenna gain is approximately -4 dBi including cable losses.

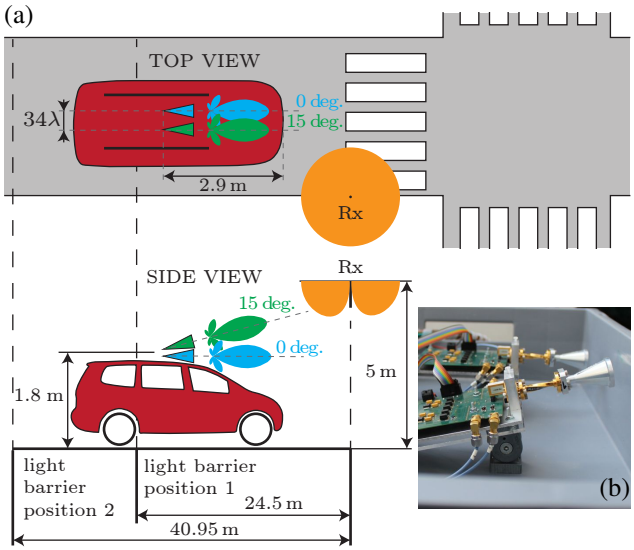

Fig. 1. (a) Measurement scenario with transmitter car, and receiver at crossroads. (b) Transmitter modules with different antenna elevation.

III. RF Setup

The hardware setup for the measurement is shown in Fig. 2. Both TXs consist of external in-phase quadrature (I/Q) mixer modules, an arbitrary waveform generator (AWG), and a frequency reference. The AWG continuously repeats a baseband sounding sequence as I/Q signal for each external I/Q-mixer module. Each I/Q-mixer up-converts the input signal to passband at 60.15 GHz center frequency with a local oscillator, synthesized by a phase-locked loop (PLL). The radio frequency outputs of the I/Q-mixers emit mmWaves through conical horn antennas. The frequency reference feeds each PLL with a 285.714 MHz reference and the AWG with a 10 MHz reference. Our receiver is a signal analyzer (SA) connected to the omni-directional antenna and a light barrier. We measure the center frequency offset (CFO) between AWG and SA at standstill before each measurement. The oscillator drift during one measurement was found to be less than 1 Hz. A measurement is started as soon as the moving transmitter vehicle passes the light barrier, which triggers the recording at the RX. We directly access the I/Q samples from the SA with a sampling rate of 125 MSamples/s.

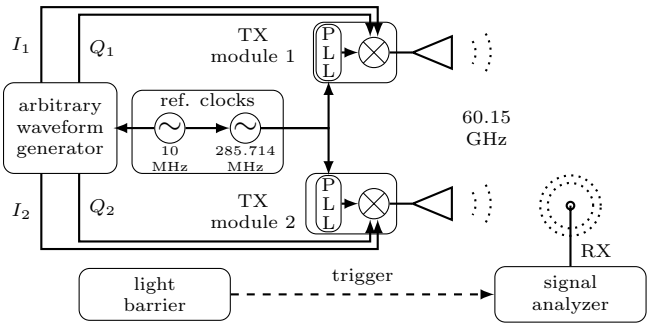

Fig. 2. Measurement setup.

IV. Sounding Sequence Design

We extract an estimate of the channel transfer function with a multitone waveform as excitation signal for channel sounding similar to the approach in [30]. A Zadoff-Chu sequence [31] is used for its constant amplitude zero autocorrelation property to keep the crest factor low and to phase-align both TXs during calibration. For our scenario, we consider a maximum excess delay $\tau_{\max}$ to the assumed propagation delay between the line of sight (LOS) component and MPCs due to single reflections. Paths due to multiple reflections and paths due to single reflections, due to back- and side-lobes at the TXs, are below the receiver sensitivity. Possible single reflections are limited by the surrounding street canyon. The width of the street canyon is 20 m. Therefore, at a maximum distance of 44 m between TXs and RX, we account for path differences between LOS and MPCs, which will not be larger than 16 m in length or 54 ns in time. Reflections at the crossing and beyond the crossing might lead to delays larger than 100 ns. The tone spacing Δf of our multitone waveform has to fulfill the sampling theorem. Therefore, $\Delta f \leq 1/(2\tau_{\max})$ needs to hold true for the maximum excess delay $\tau_{\max}$ of the channel. We use a measurement bandwidth $B = 100$ MHz and $K = 21$ tones to get a tone spacing of $\Delta f = 4.76$ MHz, which leads to a maximum alias free delay of $\tau_{\max} = 105$ ns.

To measure the channel simultaneously for our two TXs, we use a frequency division multiplexing (FDM) approach as described in [32]. We derive the multitone waveform for the second TX from the first TX with a frequency offset $\Delta f_{\text{Ant}} = 1.19$ MHz for every single tone. The superposition of both waveforms leads to a multitone-comb, so that TXs are orthogonally interleaved in frequency. The resulting multitone sounding sequence for each TX has a period of $T = 840$ ns, leaving possible additional tones unoccupied.

The snapshot time T_{snap} for the channel has to fulfill the sampling theorem for a maximum Doppler frequency $\nu_{\max}$, so that $T_{\text{snap}} \leq 1/(2\nu_{\max})$. For a maximum assumed speed of

approaching cars $v_{\max} = 14\,\mathrm{m\,s^{-1}}$, $\nu_{\max} = 2800\,\mathrm{Hz}$ and thus $T_{\text{snap}} \leq 1/(2\nu_{\max}) = 178.6\,\mu\mathrm{s}$.

The final signal-power to noise ratio (SNR) is enhanced to combat thermal noise by coherently averaging over N channel measurements up-to the maximum snapshot time. By using $N = 212$, a processing gain of $23.26\,\mathrm{dB}$ is achieved and $T_{\text{snap}} = 178.07\,\mu\mathrm{s}$ is low enough for $\nu_{\max}$.

Our RX is able to record up to $450\,\mathrm{MSamples}$ at one shot, which influences the choice of measurement bandwidth. For a sampling rate of $125\,\mathrm{MSamples/s}$, the recording time is $T_{\text{rec}} = 3.6\,\mathrm{s}$ which translates to a travel distance of $50.4\,\mathrm{m}$ at $v_{\max}$. An example of the measurement run is shown in Section VI. The parameters of the channel sounder are summarized in Table I.

TABLE I
CHANNEL SOUNDER PARAMETERS

Parameter	Value
center frequency	$f_c = 60.15\,\mathrm{GHz}$
tone spacing	$\Delta f = 4.76\,\mathrm{MHz}$
number of tones	$K = 21$
number of TX antennas	2
tone spacing between antennas	$\Delta f_{\text{Ant}} = 1.19\,\mathrm{MHz}$
bandwidth	$B = 100\,\mathrm{MHz}$
maximum alias free delay	$\tau_{\max} = 105\,\mathrm{ns}$
transmit antennas	$20\,\mathrm{dBi}$ conical horn
receive antenna	$\lambda/4$ monopole
snapshot time	$T_{\text{snap}} = 178.07\,\mu\mathrm{s}$
maximum car speed	$v_{\max} = 14\,\mathrm{m\,s^{-1}}$
recording time	$T_{\text{rec}} = 3.6\,\mathrm{s}$

V. MEASUREMENT EVALUATION

Frequency and time synchronization is performed utilizing the LOS component.

Frequency synchronization: The CFO between the oscillator of RX and TX is measured at standstill with a correlator before each measurement.

Coherent averaging: I/Q samples of the actual measurement with the car in motion are recorded. A frequency offset of the LOS due to Doppler plus CFO is estimated using correlators for each TX. We calculate the average received sounding sequence by applying a frequency offset correction and coherent averaging. The frequency correction, without the CFO, is reversed afterwards. For averaging, we use a rectangular window without overlap.

Time synchronization through LOS alignment: We estimate the propagation delay of the LOS component from the known distance between TXs at the light barrier position to the RX. Therefore, we align the delay of the LOS component accordingly.

We calculate estimates of the time-variant transfer function $H_i[t, f_i]$ similar to [7], where t is the time index $t = \{t_0, \ldots, t_{N_{\text{snap}}-1}\}$ of a snapshot and f_i are the frequency indices $f_i = \{f_{i,0}, \ldots, f_{i,K-1}\}$ selected for the given TX i due to the interleaved multitone waveform. For a total recording time $T_{\text{rec}} = 3.6\,\mathrm{s}$, the number of snapshots is $N_{\text{snap}} = 20\,275$. As common for example in OTFS modulation [28], we characterize the channel in delay-Doppler domain using a symplectic finite Fourier transform (SFFT) on $H_i[t, f_i]$. We use a multitaper based estimator within an evaluation region of M samples in time and K samples in frequency. The employed tapers are discrete prolate spheroidal sequences [33] to allow averaging of multiple independent spectral estimates of the same measurement with confinement in time and frequency. Furthermore, this type of estimator leads to delay and Doppler confined estimates. This approach is known as local scattering function (LSF) [34]–[36]. We use three tapers in time domain and three tapers in frequency domain.

From the LSF, we derive the Doppler power spectral density (DSD) as explained in [34]. For evaluation of the LSF, we set the number of snapshots to $M = 360$ and number of frequencies to $K = 21$ which corresponds to an evaluation time of $T_{\text{eval}} = 64.3\,\mathrm{ms}$ and bandwidth of $B_{\text{eval}} = 100\,\mathrm{MHz}$. In Fig. 5 and Fig. 6 we show the DSD and the LSF over the recording time.

Formalism for a sparse representation of the channel: We use the SFFT to transform consecutive time-variant frequency responses $H_i[k, l]$ into a Doppler-variant impulse response $S_i[n, m]$ and vice versa with the inverse SFFT (ISFFT). We write $H_i[k, l]$ and $S_i[n, m]$ as matrix $\mathbf{H} \in \mathbb{C}^{K\times M}$ and $\mathbf{S} \in \mathbb{C}^{K\times M}$ respectively for each i. K is the number of frequency indices k and delay indices n, and M is the number of time indices l and Doppler indices m. Splitting up the ISFFT into a discrete Fourier transform (DFT) and an inverse DFT as in [37] leads to

$$\mathbf{H} = \mathbf{F}_K \mathbf{S} \mathbf{F}_M^H \ , \tag{1}$$

where the index of the DFT matrix $\mathbf{F}$ denotes the size of the DFT. Using the *Kronecker* product $\otimes$, we find the vectorization $\mathrm{vec}(\cdot)$ of $\mathbf{H}$ as

$$\mathbf{h} = \left(\mathbf{F}_M^H \otimes \mathbf{F}_K\right) \mathbf{s} \ , \tag{2}$$

with $\mathbf{h} = \mathrm{vec}\,(\mathbf{H})$ and $\mathbf{s} = \mathrm{vec}\,(\mathbf{S})$. With the transfer matrix $\mathbf{A} = \left(\mathbf{F}_M^H \otimes \mathbf{F}_K\right)$ and additive noise $\mathbf{w}$, $\mathbf{h}$ is expressed as

$$\mathbf{h} = \mathbf{A}\mathbf{s} + \mathbf{w} \ , \tag{3}$$

where we want to find a vector $\hat{\mathbf{s}}$ which is a sparse representation of the measured channel. In this contribution a sparse fit is obtained with two different methods.

Largest peaks of LSF: We find a sparse fit through trivial two-dimensional peak search of the LSF and selection of the ten largest peaks.

Sparse fit using SBL: Moreover, we find a sparse representation of the channel $\mathbf{h}$ with the SBL algorithm in [25] as a solver. Based on $\mathbf{F}_K$, we define a DFT matrix $\tilde{\mathbf{F}}_K \in \mathbb{C}^{K\times 4K}$ for super-resolution in the delay domain by a factor of 4. This enhances the resolution of the estimation, which is given by the channel sounder's sampling in frequency. The modified transfer matrix for the solver is then $\tilde{\mathbf{A}} = \mathbf{F}_M^H \otimes \tilde{\mathbf{F}}_K \in \mathbb{C}^{KM\times 4KM}$, which leads to the model

$$\mathbf{h} = \tilde{\mathbf{A}}\tilde{\mathbf{s}} + \mathbf{w} \ , \tag{4}$$

with $\tilde{\mathbf{s}} \in \mathbb{C}^{4KM}$, the resolution enhanced version of $\mathbf{s}$. Instead of $\tilde{\mathbf{s}}$, SBL iteratively estimates the channel powers through the

variances $\boldsymbol{\gamma} = [\gamma_1, \ldots, \gamma_{4KM}]^T$. Furthermore, each iteration in SBL estimates the noise variance based on active set selection using the P largest peaks in $\boldsymbol{\gamma}$. We modify the one-dimensional selection in [25] for a two-dimensional peak selection in $\mathrm{vec}^{-1}(\boldsymbol{\gamma}) \in \mathbb{R}^{4K \times M}$ according to our delay-Doppler plane. For the SBL algorithm, we use the SBL1 variant in [25] and $P = 10$. Initial channel variances are $\boldsymbol{\gamma} = [1, \ldots, 1]^T$ and initial noise variance is 0.1. Ten iterations are done.

VI. Results

Fig. 3. Our transmitter car passing through the measurement scenario. The car triggers the recording by passing the light barrier. Within the first second of the recording, additional multipath components (MPCs) exist due to a parked truck, which contribute to fading. Those MPCs no longer exist after the car passes the truck at 2 s. The car passes the receiver near 3 s.

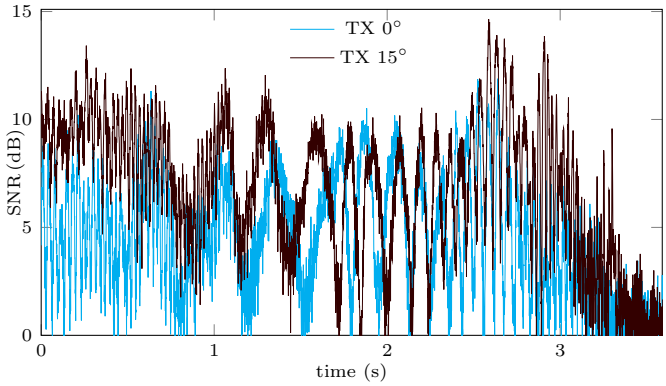

Fig. 4. The receiver SNR per transmitter for the measurement example. Additional MPCs in the first third of the recording cause stronger fading for TX 0° and more SNR for TX 15°. Both TXs show similar SNR in the second third because fading is dominated by two signal paths. In the last third, the elevated TX 15° shows a short soar in SNR compared to TX 0° due to the spatial filtering. The SNR drops quickly for both TXs as the car approaches the area below the receiver.

As an example, we show a measurement in Fig. 3 with the transmitter car passing through the whole measurement scenario at constant speed. The recording is triggered when the car passes the light barrier 41 m before the RX position. The car continues towards the crossroads without stopping at the green traffic light and then passes the RX. The SNR at the RX is shown in Fig. 4. Fading is different for both TX antennas.

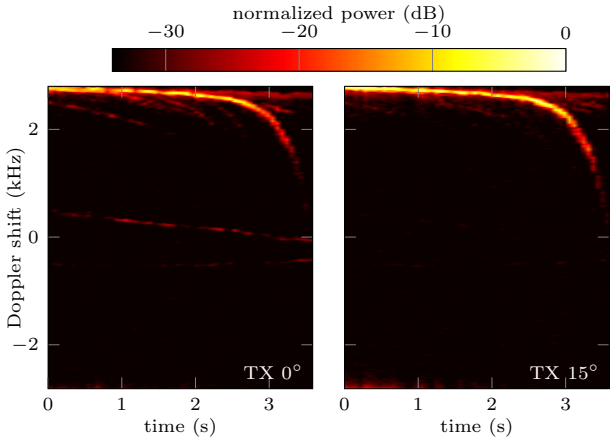

Fig. 5. Doppler power spectral density of the measurement example. At 0 s, the LOS has a Doppler-shift of more than 2.5 kHz. The LOS dominates the wireless channel in the Doppler domain equally for both TXs. The TX 15° shows fewer MPCs due to spatial filtering of the street level. Doppler-shift of the LOS moves towards negative frequencies due to change in radial velocity as the car passes the receiver.

Fading through MPCs in the first third of the recording is due to a parked truck. In the second third, fading is equal for both TX antennas because only two dominant signal paths exist. As the car passes the RX, SNR decreases first for the horizontal beam and later for the elevated beam due to spatial filtering. The Doppler power spectral density is shown in Fig. 5 with a dominant LOS component. The elevated beam shows fewer MPCs due to spatial filtering of the street level. For both antenna elevations, a LOS component with Doppler shift of more than 2.5 kHz is visible at 0 s. As the car approaches the RX, Doppler shift of the LOS component decreases towards negative frequencies.

The channel power spreading in delay-Doppler domain, over the course of the measurement, is shown in Fig. 6. The spreading is mostly limited to a cluster around the LOS component and is thus described as a sparse channel in the delay-Doppler domain. Components arriving before the LOS are due to the previously mentioned reflections beyond the crossing (aliasing), and DFT leakage. Results from the sparse channel estimation with SBL are shown in Fig. 6. They are in good agreement with the peaks of the LSF. Furthermore, finer sampling in the delay domain reveals additional MPCs.

VII. Conclusion

The measured V2I wireless channels in an urban environment are dominated by one cluster in the delay-Doppler domain. In a communication system, this allows for easy compensation for delay and Doppler shifts of the whole cluster, and enables the design of low-complexity receivers. This type of channel is especially suitable for OTFS modulation. Both considered beam elevations of the antennas at the car's roof have only a weak impact on the V2I channel in delay-Doppler domain. However, the elevated beam is less subject to fading due to weaker illumination of the street level. SBL is able to find a sparse representation of the measured channel, which agrees with results from the LSF, and reveals additional MPCs.

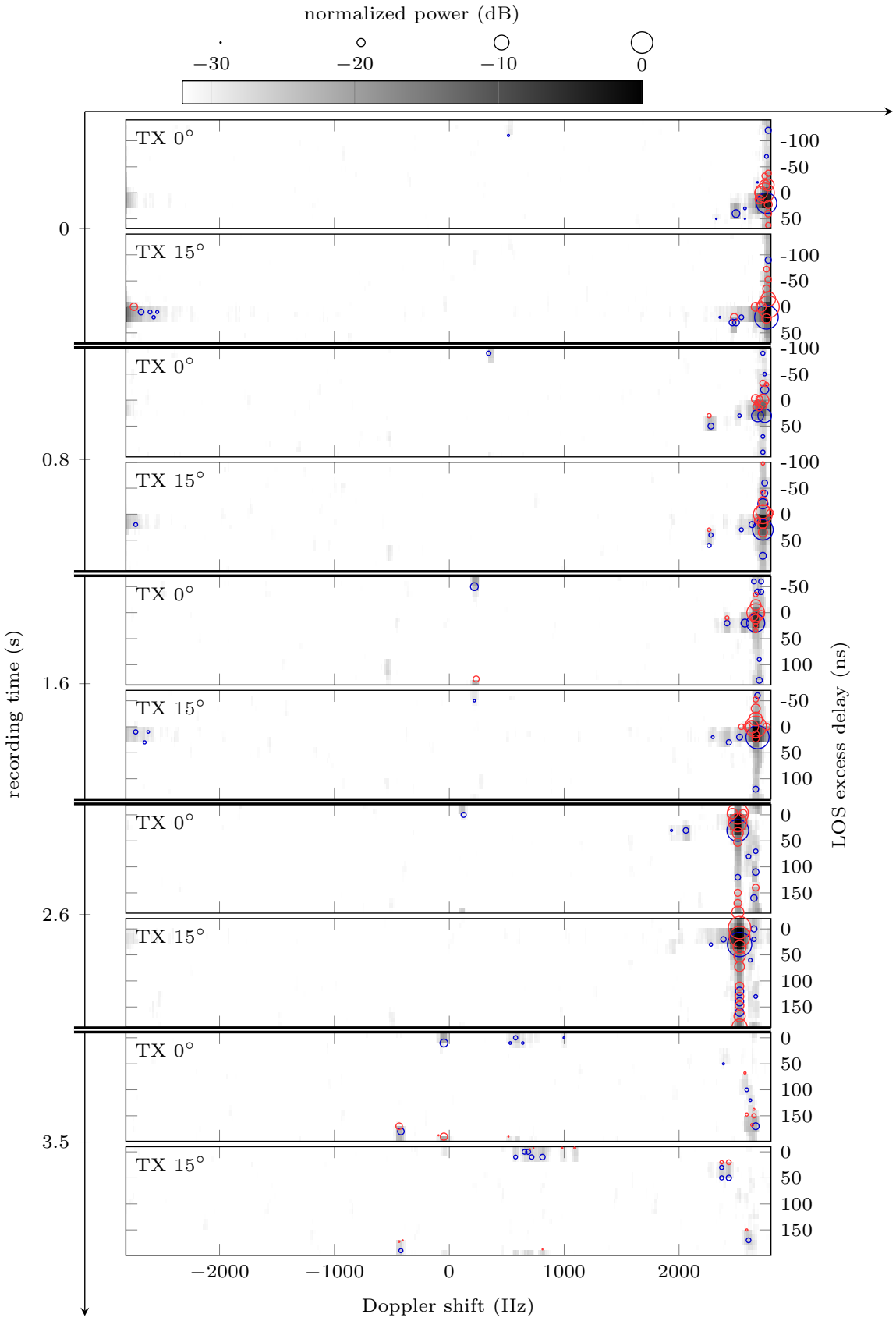

Fig. 6. Spreading of channel power in the delay-Doppler domain for each transmitter. The delay is with respect to the LOS component. The ten largest peaks are shown as blue circles for the local scattering function (LSF), and red circles for the sparse Bayesian learning (SBL) results based on ten iterations. The wireless channel is dominated by a single cluster in the delay-Doppler domain at the LOS component. The SBL results agree with the largest peaks of the LSFs. Two strong paths with equal Doppler but different delay are resolved by SBL, e.g. at 2.6 s recording time.

References

[1] L. Cheng, B. E. Henty, D. D. Stancil, F. Bai, and P. Mudalige, "Mobile vehicle-to-vehicle narrow-band channel measurement and characterization of the 5.9 GHz dedicated short range communication (DSRC) frequency band," *IEEE Journal on Selected Areas in Communications*, vol. 25, no. 8, 2007.

[2] O. Renaudin, V.-M. Kolmonen, P. Vainikainen, and C. Oestges, "Wideband MIMO car-to-car radio channel measurements at 5.3 GHz," in *Proc. of the IEEE 68th Vehicular Technology Conference (VTC-Fall)*, 2008.

[3] A. Paier, J. Karedal, N. Czink, C. Dumard, T. Zemen, F. Tufvesson, A. F. Molisch, and C. F. Mecklenbräuker, "Characterization of vehicle-to-vehicle radio channels from measurements at 5.2 GHz," *Wireless Personal Communications*, vol. 50, no. 1, pp. 19–32, 2009.

[4] C. F. Mecklenbräuker, A. F. Molisch, J. Karedal, F. Tufvesson, A. Paier, L. Bernadó, T. Zemen, O. Klemp, and N. Czink, "Vehicular channel characterization and its implications for wireless system design and performance," *Proceedings of the IEEE*, vol. 99, no. 7, pp. 1189–1212, 2011.

[5] H. Meinel and A. Plattner, "Millimetre-wave propagation along railway lines," *IEE Proceedings F-Communications, Radar and Signal Processing*, vol. 130, no. 7, pp. 688–694, 1983.

[6] A. Kato, K. Sato, M. Fujise, and S. Kawakami, "Propagation characteristics of 60-GHz millimeter waves for ITS inter-vehicle communications," *IEICE Transactions on Communications*, vol. 84, no. 9, pp. 2530–2539, 2001.

[7] E. Zöchmann *et al.*, "Measured delay and Doppler profiles of overtaking vehicles at 60 GHz," 2018.

[8] J. Blumenstein *et al.*, "Measured high-resolution power-delay profiles of nonstationary vehicular millimeter wave channels," in *Proc. of the IEEE 29th Annual International Symposium on Personal, Indoor and Mobile Radio Communications (PIMRC)*, 2018.

[9] E. Zöchmann *et al.*, "Statistical evaluation of delay and Doppler spread in 60 GHz vehicle-to-vehicle channels during overtaking," in *Proc. of the IEEE-APS Topical Conference on Antennas and Propagation in Wireless Communications (APWC)*, 2018.

[10] ——, "Position-specific statistics of 60 GHz vehicular channels during overtaking," *IEEE Access*, pp. 1–17, 2019, early access.

[11] M. G. Sánchez, M. P. Táboas, and E. L. Cid, "Millimeter wave radio channel characterization for 5G vehicle-to-vehicle communications," *Measurement*, vol. 95, pp. 223–229, 2017.

[12] A. Prokeš *et al.*, "Time-domain broadband 60 GHz channel sounder for vehicle-to-vehicle channel measurement," in *Proc. of the IEEE Vehicular Networking Conference (VNC)*, 2018.

[13] J.-J. Park, J. Lee, K.-W. Kim, M.-D. Kim, and K. C. Lee, "28 GHz Doppler measurements in high-speed expressway environments," in *Proc. of the IEEE 29th Annual International Symposium on Personal, Indoor and Mobile Radio Communications (PIMRC)*, 2018.

[14] A. Prokes, J. Vychodil, M. Pospisil, J. Blumenstein, T. Mikulasek, and A. Chandra, "Time-domain nonstationary intra-car channel measurement in 60 GHz band," in *Proc. of the International Conference on Advanced Technologies for Communications (ATC)*, 2016.

[15] J. Blumenstein, A. Prokes, J. Vychodil, M. Pospisil, and T. Mikulasek, "Time-varying K factor of the mm-wave vehicular channel: Velocity, vibrations and the road quality influence," in *Proc. of the IEEE 28th Annual International Symposium on Personal, Indoor, and Mobile Radio Communications (PIMRC)*, 2017.

[16] A. M. Sayeed and V. Raghavan, "Maximizing MIMO capacity in sparse multipath with reconfigurable antenna arrays," *IEEE Journal of Selected Topics in Signal Processing*, vol. 1, no. 1, pp. 156–166, 2007.

[17] C. Gustafson, K. Haneda, S. Wyne, and F. Tufvesson, "On mm-wave multipath clustering and channel modeling," *IEEE Transactions on Antennas and Propagation*, vol. 62, no. 3, pp. 1445–1455, 2014.

[18] E. Zöchmann, S. Caban, C. F. Mecklenbräuker, S. Pratschner, M. Lerch, S. Schwarz, and M. Rupp, "Better than Rician: modelling millimetre

[19] K. Venugopal, A. Alkhateeb, N. G. Prelcic, and R. W. Heath, "Channel estimation for hybrid architecture-based wideband millimeter wave systems," *IEEE Journal on Selected Areas in Communications*, vol. 35, no. 9, pp. 1996–2009, 2017.

wave channels as two-wave with diffuse power," *EURASIP Journal on Wireless Communications and Networking*, vol. 2019, no. 1, pp. 1–21, 2019.

[20] T. Blazek and C. F. Mecklenbräuker, "Sparse time-variant impulse response estimation for vehicular channels using the c-LASSO," in *Proc. of the IEEE 28th Annual International Symposium on Personal, Indoor, and Mobile Radio Communications (PIMRC)*, 2017.

[21] T. Blazek, E. Zöchmann, and C. F. Mecklenbräuker, "Approximating clustered millimeter wave vehicular channels by sparse subband fitting," in *Proc. of the IEEE 29th Annual International Symposium on Personal, Indoor and Mobile Radio Communications (PIMRC)*, 2018.

[22] ——, "Model order selection for LASSO fitted millimeter wave vehicular channel data," in *Proc. of the IEEE 29th Annual International Symposium on Personal, Indoor and Mobile Radio Communications (PIMRC)*, 2018.

[23] T. Blazek, E. Zöchmann, and C. Mecklenbräuker, "Millimeter wave vehicular channel emulation: A framework for balancing complexity and accuracy," *Sensors*, vol. 18, no. 11, p. 3997, 2018.

[24] R. Prasad, C. R. Murthy, and B. D. Rao, "Joint approximately sparse channel estimation and data detection in OFDM systems using sparse Bayesian learning." *IEEE Transactions on Signal Processing*, vol. 62, no. 14, pp. 3591–3603, 2014.

[25] P. Gerstoft, C. F. Mecklenbräuker, A. Xenaki, and S. Nannuru, "Multi-snapshot sparse Bayesian learning for DOA," *IEEE Signal Processing Letters*, vol. 23, no. 10, pp. 1469–1473, 2016.

[26] H. Groll, C. F. Mecklenbräuker, and P. Gerstoft, "Sparse Bayesian learning for directions of arrival on an FPGA," in *Proc. of the IEEE Statistical Signal Processing Workshop (SSP)*, 2018.

[27] G. Tauböck and F. Hlawatsch, "A compressed sensing technique for OFDM channel estimation in mobile environments: Exploiting channel sparsity for reducing pilots," in *Proc. of the IEEE International Conference on Acoustics, Speech and Signal Processing (ICASSP)*, 2008.

[28] R. Hadani, S. Rakib, M. Tsatsanis, A. Monk, A. J. Goldsmith, A. F. Molisch, and R. Calderbank, "Orthogonal time frequency space modulation," in *Proc. of the IEEE Wireless Communications and Networking Conference (WCNC)*, 2017.

[29] R. Hadani, S. Rakib, A. Molisch, C. Ibars, A. Monk, M. Tsatsanis, J. Delfeld, A. Goldsmith, and R. Calderbank, "Orthogonal time frequency space (OTFS) modulation for millimeter-wave communications systems," in *Proc. of the IEEE MTT-S International Microwave Symposium (IMS)*, 2017.

[30] S. Sangodoyin, J. Salmi, S. Niranjayan, and A. F. Molisch, "Real-time ultrawideband MIMO channel sounding," in *Proc. of the 6th European Antennas and Propagation Conference (EuCAP)*, 2012.

[31] D. Chu, "Polyphase codes with good periodic correlation properties (corresp.)," *IEEE Transactions on information theory*, vol. 18, no. 4, pp. 531–532, 1972.

[32] Y. Konishi, M. Kim, M. Ghoraishi, J. Takada, S. Suyama, and H. Suzuki, "Channel sounding technique using MIMO software radio architecture," in *Proc. of the 5th European Conference on Antennas and Propagation (EuCAP)*, 2011.

[33] D. Slepian, "Prolate spheroidal wave functions, Fourier analysis, and uncertainty–V: The discrete case," *Bell System Technical Journal*, vol. 57, no. 5, pp. 1371–1430, 1978.

[34] L. Bernadó, T. Zemen, F. Tufvesson, A. F. Molisch, and C. F. Mecklenbräuker, "Delay and Doppler spreads of nonstationary vehicular channels for safety-relevant scenarios," *IEEE Transactions on Vehicular Technology*, vol. 63, no. 1, pp. 82–93, 2014.

[35] ——, "Time-and frequency-varying K-factor of non-stationary vehicular channels for safety-relevant scenarios," *IEEE Transactions on Intelligent Transportation Systems*, vol. 16, no. 2, pp. 1007–1017, 2015.

[36] D. J. Thomson, "Spectrum estimation and harmonic analysis," *Proceedings of the IEEE*, vol. 70, no. 9, pp. 1055–1096, 1982.

[37] A. Rezazadeh Reyhani, A. Farhang, M. Ji, R. R. Chen, and B. Farhang-Boroujeny, "Analysis of discrete-time MIMO OFDM-based orthogonal time frequency space modulation," in *Proc. of the IEEE International Conference on Communications (ICC)*, 2018.